Bull. Mater. Sci., Vol. 36, No. 1, February 2013, pp. 51–58. © Indian Academy of Sciences.

Electrochemical passivation behaviour of nanocrystalline $Fe_{80}Si_{20}$ coating in borate buffer solution

G GUPTA, A P MOON and K MONDAL*
Department of Materials Science and Engineering, Indian Institute of Technology, Kanpur 208 016, India

MS received 7 November 2011; revised 8 April 2012

Abstract. **Passivation behaviour of nanocrystalline coating ($Fe_{80}Si_{20}$) obtained by *in situ* mechanical alloying route is studied and compared with that of the commercial pure iron and cast $Fe_{80}Si_{20}$ in sodium borate buffer solution at two different pH values (7·7 and 8·4). The coating reveals single passivation at a pH of 7·7 and double stage passivity at a pH of 8·4. The first passive layer is due to the dissolution mechanism and second passivity is related to stable passivation. The cast sample shows single stage passivity in the solution of pH 8·4. The difference in the passivation behaviour for the cast alloy ($Fe_{80}Si_{20}$) and the coating is related to the presence of highly iron-enriched localized regions, formed during the processing stage of coating.**

Keywords. **Coatings; passive layer; polarization; scanning electron microscope.**

1. Introduction

Nanocrystalline coatings have gained significant interest due to their unique mechanical, electrochemical and physical properties (Suryanarayana and Koch 2000; Froes *et al* 2001; Tjong and Chen 2004). Though the mechanical behaviour of nanocrystalline materials have been studied extensively, interests in the investigation on its electrochemical and corrosion behaviour in aqueous media are gaining importance due to the potential application of nanocrystalline materials as coating. Both beneficial as well as detrimental effects of the nanocrystalline coatings have been reported and the properties of coating can be influenced by many factors such as grain size and its distribution, surface condition, adherence to the substrate, reactivity with the medium and its preparation routes, etc (Szewieczek *et al* 1998; Huang *et al* 2002; Ji *et al* 2005; Ghosh *et al* 2006; Lu *et al* 2006; Meng *et al* 2006; Wang *et al* 2006).

Several studies have been conducted in the past to investigate electrochemical corrosion and passivation behaviour of nanocrystalline coatings such as study of Fe–10Cr nanocrystalline coating produced by magnetron sputtering on glass slides in 0·05 M H_2SO_4 + 0·25 M Na_2SO_4 and 0·05 M H_2SO_4 + 0·5 M NaCl solution. It has been reported that the active dissolution rate of the coating is higher as compared to the cast alloy and higher Cr content in the passive layer has led to the passivation of the coating (Meng *et al* 2006). The improved chemical stability and repassivation ability of the passive film on the coating have attributed to the lower donor density and increased Cr content in the passive film. Corrosion resistance of another nanocrystalline coating made of $Fe_{73·5}Cu_1Nb_3Si_{13·5}B_9$ alloy has been studied and found to be higher than amorphous counterpart in acidic solutions (Szewieczek *et al* 1998). These results attribute to the presence of a specific volume fraction of nanocrystalline α-Fe (Si) phase and interfacial grain boundary phase. Corrosion behaviour of high velocity oxygen fuel (HVOF) sprayed nanocrystalline coating of $Fe_{60}Al_{40}$ has been compared with the extruded samples of same composition in H_2SO_4 solution (Ji *et al* 2005). It has been found that the corrosion resistance of the coating is poor and these results attribute to the preferential attack at the interconnected porosities at intersplat boundaries without much change in the active–passive state. Nanocrystalline nickel coating made by pulsed electrodeposition in alkaline media (10 wt% NaOH) (Wang *et al* 2006) shows that there is an increase in corrosion resistance with the decrease in the grain size and this is related to the rapid formation of continuous $Ni(OH)_2$ passive film at crystalline defects on the surface. It is clear that depending on the composition, grain size, morphology, solution interaction of active species, etc. there could be either enhancement or decrease in the corrosion resistance of the coating.

Fe–Si alloys possess excellent soft magnetic properties like low coercivity and high magnetic saturation that make them suitable as magnetic components like transformer magnets, magnetic cores, etc (Ding *et al* 2001; Li and Li 2010). The passivation behaviour of binary cast Fe–Si alloys tested in phthalate buffer solution has shown that low Si alloys do not form a thick SiO_2 layer and only iron oxide layer forms. In case of Si-rich alloys, formation of a stable SiO_2 layer leads to improved corrosion resistance (Wolff *et al* 2001). The stability of the passive layer is improved in case of high Si content alloys (more than 21·3 at% Si) due to the formation of Fe_3Si phase from α-Fe. Another study (Omurtag and Doruk 1970) has shown that the passive behaviour of a number of cast Fe–Si binary alloys in H_2SO_4 at 25 °C

*Author for correspondence (kallol@iitk.ac.in)

is controlled by the iron oxide film in case of alloys with Si content less than 14 (wt%); whereas, it is controlled by SiO_2 film when the Si content is 14%. The corrosion studies on the bulk Fe–Si alloys have been reported (Omurtag and Doruk 1970; Wolff *et al* 2001) but there are not many specific studies related to the corrosion of nanocrystalline Fe–Si alloys.

In the present case, electrochemical studies of adherent and thick nanocrystalline $Fe_{80}Si_{20}$ (at %) coating of 200 μm thick made by *in situ* ball milling are carried out (Gupta *et al* 2009). The passivation behaviour of the nanocrystalline $Fe_{80}Si_{20}$ coating is also tested in sodium borate buffer solutions in comparison with that of commercially pure iron and cast alloy of same composition. Reasons for possible difference in polarization behaviour of iron and cast $Fe_{80}Si_{20}$ alloy and the coating are discussed on the basis of surface morphology and nanocrystalline structure.

2. Experimental

Nanocrystalline ($Fe_{80}Si_{20}$) alloy was prepared by ball milling pure elemental powders of Fe and Si in Retsch planetary ball mill (PM400) for 20 h at a speed of 300 rpm in toluene medium used as process control agent. The balls and vial were made of stainless steel and the ball to powder ratio was maintained at 10:1. Coupons (15 mm × 15 mm × 3 mm) of mild steel were prepared and polished to 15 μm finish using SiC emery papers and then progressively fine-polished from 5 μm to 1 μm surface finish using alumina slurry on velvet cloth. The samples were ultrasonically cleaned with acetone for 5 min. Coupons were dry-milled with the nanocrystalline alloy powder at a speed of 200 rpm to obtain the coating of nanocrystalline $Fe_{80}Si_{20}$ on the mild steel substrate. Cast Fe–Si alloy of the same composition was prepared by arc melting

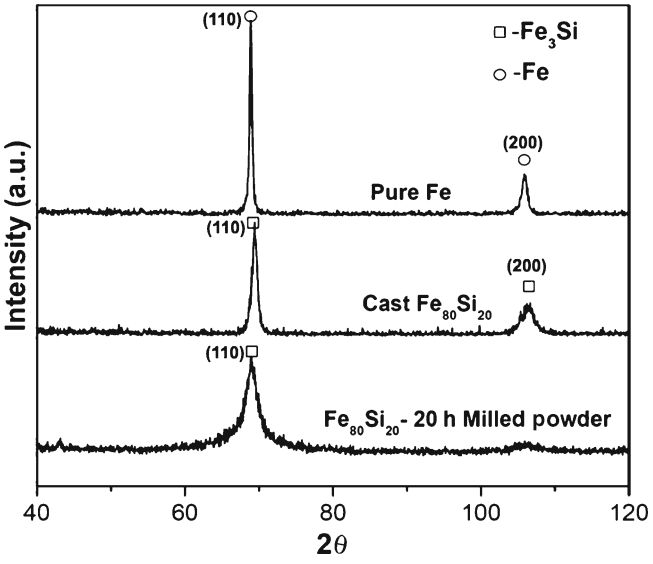

Figure 1. XRD patterns of $Fe_{80}Si_{20}$ powder milled for 20 h, cast $Fe_{80}Si_{20}$ and pure Fe.

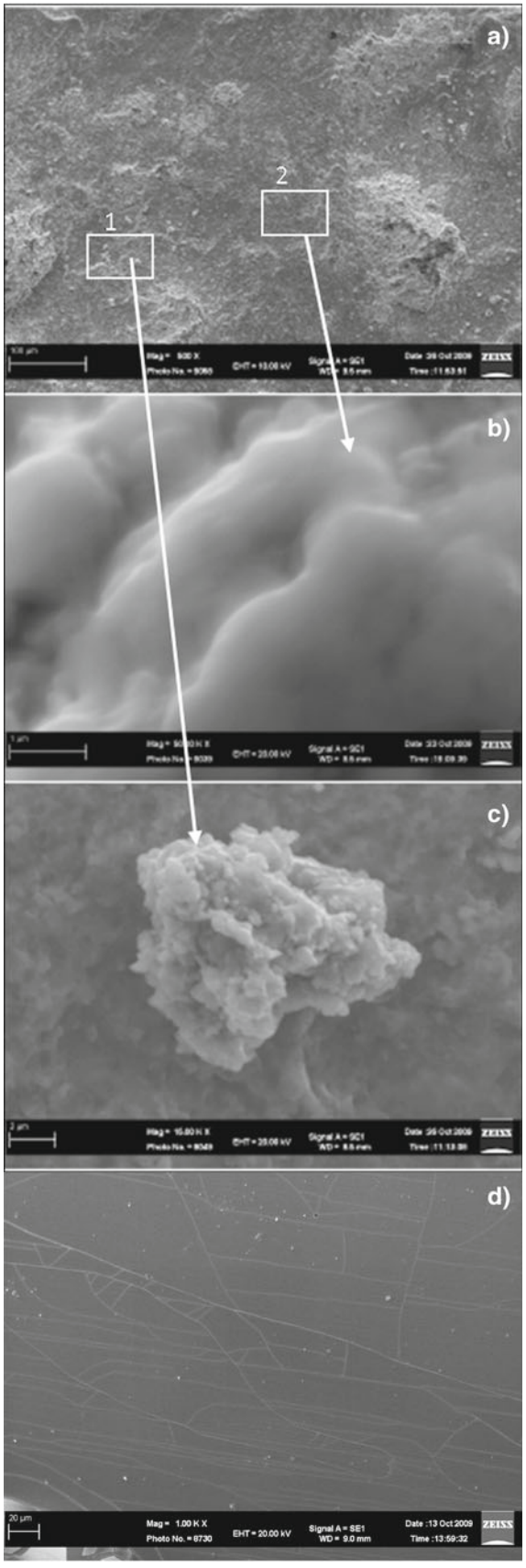

Figure 2. (**a–c**) Scanning electron micrographs showing microstructure before electrochemical testing for coating and (**d**) cast $Fe_{80}Si_{20}$.

pure Fe and Si of 99·9% purity. Coupons of 8 × 8 × 1 mm were cut from cast samples and commercially pure iron using a diamond cutter and polished to 15 μm surface finish using SiC emery papers and then fine-polished progressively to 1 μm using alumina slurry on velvet cloth. Nanocrystalline $Fe_{80}Si_{20}$ alloy powder, as-cast Fe–Si alloy samples and pure iron were analysed using X-ray diffraction (XRD) with a Rich Seifert 2000D diffractometer using CrKα radiation to understand the phases present in the alloy.

All the samples were ultrasonically cleaned using acetone for 5–10 min before performing electrochemical tests. The corrosion behaviour of the substrate and the coating was studied in freely-aerated borate buffer solution ($Na_2B_4O_7 \cdot 10H_2O$ 19·069 g/l, KNO_3 1·010 g/l and H_3BO_3 30·915 g/l) at two different pH values (pH 7·7 and pH 8·4) by potentiodynamic polarization in a potentiostat (Model 2263, Princeton applied research, USA) at an ambient temperature (25–28°C) at a scan rate of 0·166 mV/s. The pH of the solution has been chosen so as to observe the effect of Si in the alloy, as pH 7·7 lies in active–passive region and pH 8·4 lies in the complete passive region for Fe (Pourbaix 1966). However, Si is completely passive in all the pH values as evident from Pourbaix diagrams (Pourbaix 1966). Thus, the two different pH values are chosen to understand the effect of Si on the passivity of Fe–Si alloy. The pH of the borate buffer solution was adjusted by adding drops of 2 M NaOH solution. The electrochemical experiments were performed in a flat cell (Princeton applied research, USA) using saturated calomel electrode (E_{SCE} = +241 mV with respect to standard hydrogen electrode (SHE)) as reference electrode and platinum as the counter electrode. The surface area exposed to the solution in case of coatings and mild steel was 1 cm^2 and 0·5 cm^2 for pure Fe and cast $Fe_{80}Si_{20}$ samples, respectively. All the calculations were normalized with respect to area. All the experiments were conducted after stabilization of free corrosion potential (FCP) such that the variation in potential was less than 5 mV in 10 min. Potentiodynamic polarization experiments were conducted in the range of 250 mV below FCP to 1·6 V at a scan rate of 0·166 mV/s. Electrochemical tests were also performed on as-cast Fe–Si alloy and pure Fe samples in freely-aerated borate buffer solution (pH-8·4). The surfaces of the coated samples and as-cast samples before and after electrochemical tests were studied using scanning electron microscopy (Carl Zeiss-EVO 50). The compositions were obtained with the help of energy dispersive spectroscopy (EDS). The average composition was attained from 10 to 15 measurements in the scanned area.

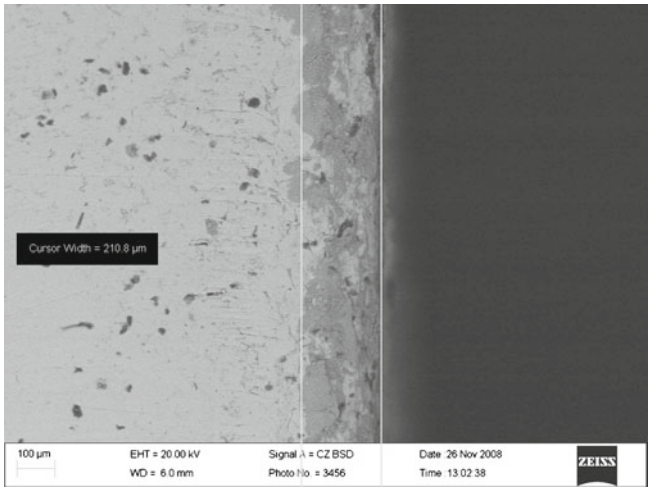

Figure 3. Backscattered SEM micrograph of cross section of *in situ* coating made at 200 rpm for 1 h by milling alloy powder and substrate together.

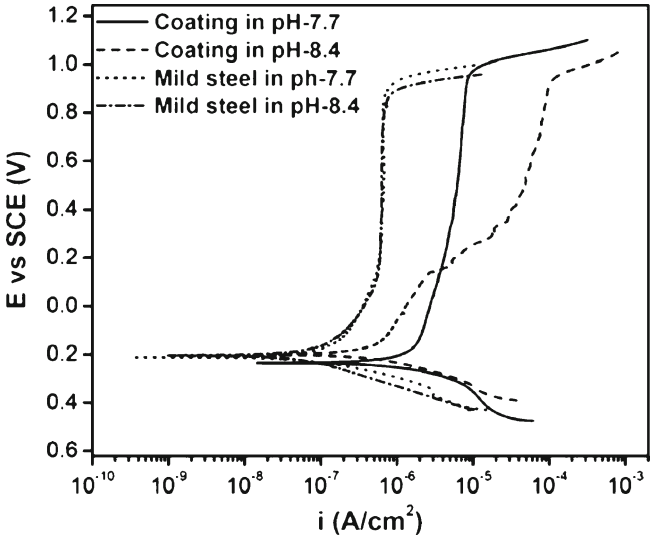

Figure 4. Potentiodynamic polarization plots for mild steel substrate and coating in borate buffer solution of pH-7·7 and pH-8·4.

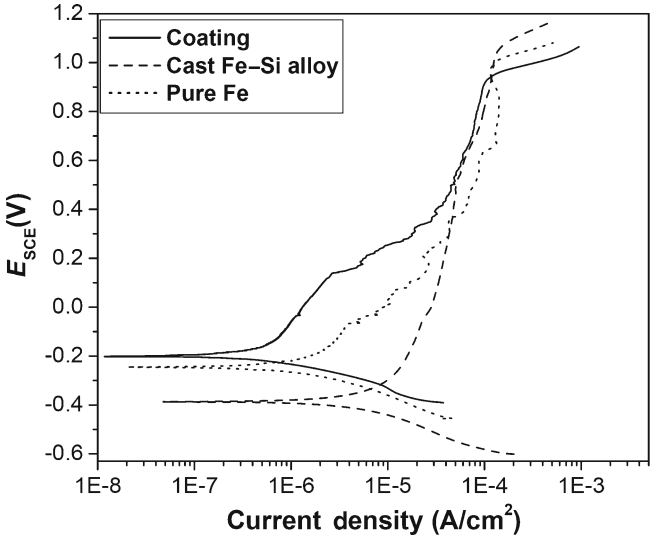

Figure 5. Potentiodynamic polarization plot for coating, cast Fe–Si alloy and pure Fe in borate buffer solution of pH-8·4.

3. Results

Figure 1 shows XRD patterns of the $Fe_{80}Si_{20}$ powder which has been used for coating material on mild steel, cast $Fe_{80}Si_{20}$ alloy and pure iron. Diffraction peaks in figure 1 are identified as the α-Fe peaks (*bcc*) in case of pure iron with reflection from planes (110) and (200) respectively. The as-cast alloy $Fe_{80}Si_{20}$ reveals Fe_3Si peaks with reflection from planes (110) and (200). The line broadening arises due to the reduction of the grains size and crystallite size is estimated to be 17 nm (Gupta *et al* 2009) and increase in the internal strains induced due to the repetitive fracture and cold welding processes during milling. The peak for pure iron as well as cast alloy are intense whereas broader peaks could be seen in case of milled powder indicating the grain size of these materials to be smaller than that of the pure iron and cast alloy. Figure 2(a–c) shows SEM micrographs of the coating and figure 2(d) shows the SEM micrograph of the cast $Fe_{80}Si_{20}$ alloy. There are resemblance of island type structure on the surface of the coating and regions 1 and 2 of figure 2(a) which are further magnified to reveal the structure at different areas of the island. There are two types of regions present on the surface: one consists of agglomerates of the embedded particles of the Fe–Si alloy and the other is cold welded structure of the alloy along with iron rich regions. The cold welding between the particles of the alloy and the agglomeration of different particles are shown in figures 2(b) and (c), respectively. EDX spectrum as obtained from the surface shown from the points denoted as A and B in figures 2(b) and (c), respectively, indicates the presence of Fe-24 at% Si regions and pure Fe (EDX spectrum not shown). The particle size is approximately 0·5–1 μm. The microstructure of the cast alloy reveals the grain boundaries present on the surface and it can be clearly seen that the grains are elongated.

Figure 3 shows SEM backscattered micrograph obtained from cross-sectional surface of the coating. The interface is rough in nature as compared to the external coated surface. The bright regions signify the substrate and the dark regions represent the coating. It is clearly visible that some of the bright regions are occluded by the gray region and *vice-versa*. So, it can be said that during initial stages of ball milling, some of the substrate is being chipped off which results in the formation of rough interface. The chipped-off region is not completely separated but redeposited back with further milling that results in the formation of coating with some iron enriched regions. It has already been reported that the coating mechanism comprises of three steps i.e. repeated impact, cold welding followed by delamination (Gupta *et al* 2009). It has also been observed by EDX analysis that some amount of Si is also present in the bright regions which is the result of inter-diffusion. The percentage of Si reduces as we move from the edge of the coating to the interface.

Figure 4 shows potentiodynamic polarization curves for the substrate and the coating in borate buffer solutions and they indicate passive characteristics. The current density in the anodic polarization region increases at potential (E_{O2}) which is similar (about 970 mV_{SCE}) in both the solutions for the coating and this potential corresponds to oxygen evolution. The passive layer in case of the substrate for both the solutions and the coating in pH-7·7 solution is stable over the entire range of anodic potential prior to oxygen evolution reaction. However, the formation of two different passive layers is observed in case of coating in the solution of pH 8·4 with a dissolution region and the potential is termed as E_d. The passive current density for the substrate (0·7 $\mu A/cm^2$) is much lower as compared to the coating in both solutions. The passive current density (i_{pass}) in case of pH-7·7 (30 $\mu A/cm^2$) is higher than that of the first passive layer (1 $\mu A/cm^2$) in the solution of pH-8·4. However, i_{pass} of the second passive layer is higher by almost two orders of magnitude (80 $\mu A/cm^2$) than that of the first one.

Figure 5 compares the potentiodynamic polarization curves of the coating, cast Fe–Si alloy and pure iron in borate buffer solution of pH-8·4. A stable passive layer observed in the entire range of anodic polarization before breakdown corresponding to oxygen evolution (E_b) at 1·02 V_{SCE} in case of cast alloy. The i_{pass} of the cast Fe–Si alloy is higher (10 $\mu A/cm^2$) in comparison to first passive layer and same as that of the second passive layer of the coating. The behaviour of pure iron is similar to the coating; it has two passive layers and a dissolution region in between two passive layers. The i_{pass} of pure Fe for first passive layer (1 $\mu A/cm^2$) is of the same order as compared to that of the coating and its value is less as compared to that of the cast alloy. However, the i_{pass}

Table 1. Parameters obtained from free corrosion potential measurements and potentiodynamic polarization curves for coating, cast Fe–Si and pure Fe in borate buffer solution at different pH values.

Sample	Solution	FCP (mV vs SCE)	ZCP (mV vs SCE)	β_c (mV/dec)	I_{pass1} ($\mu A/cm^2$)	E_{pit} (mV vs SCE)	I_{pass2} ($\mu A/cm^2$)	E_b (mV vs SCE)	E_b (mV vs SCE)
Mild Steel	Borate buffer pH-7·7	−200	−205	80	0·6	–	–	900	1017
Coating		−160	−180	140	28	–	–	970	1017
Mild steel	Borate buffer pH-8·4	−180	−204	110	0·6	–	–	890	976
Coating		−140	−200	90	1	−140	80	968	976
Cast Fe–Si		−350	−390	135	10	–	–	1020	976
Pure Fe		−200	−240	150	1	−70	30	980	976

for second passive layer (30 μA/cm^2) increases as compared to cast alloy and it is slightly higher in comparison to that of the coating. Table 1 lists all the parameters obtained from the polarization curves for the coating in the solution of pH 7·7 and 8·4, cast Fe–Si and pure Fe in the borate buffer solution of pH 8·4. E_{corr} is defined at the corrosion potential and corresponds to the potential at which the cathodic and anodic reactions are in equilibrium and the net current density is close to zero. β_c is defined as the Tafel cathodic constant which is obtained by applying Tafel equation to the polarization curve. E_{pit} is defined as the potential corresponding to the start of dissolution region or the failure of 1st passive layer. E_b is defined as the potential corresponding to oxygen evolution reaction.

Figure 6(a) shows SEM micrograph of the corroded surface of the coating in the borate buffer solution of pH-7·7. Regions with different contrast are visible on the surface due to different compositions. It is interesting to note that there are regions of pure Fe and preferably Fe-rich regions on the surface as confirmed by EDX (table 2). During initial stages of coating some part of the mild steel substrate is chipped off from the interface. The chipped-off part does not separate

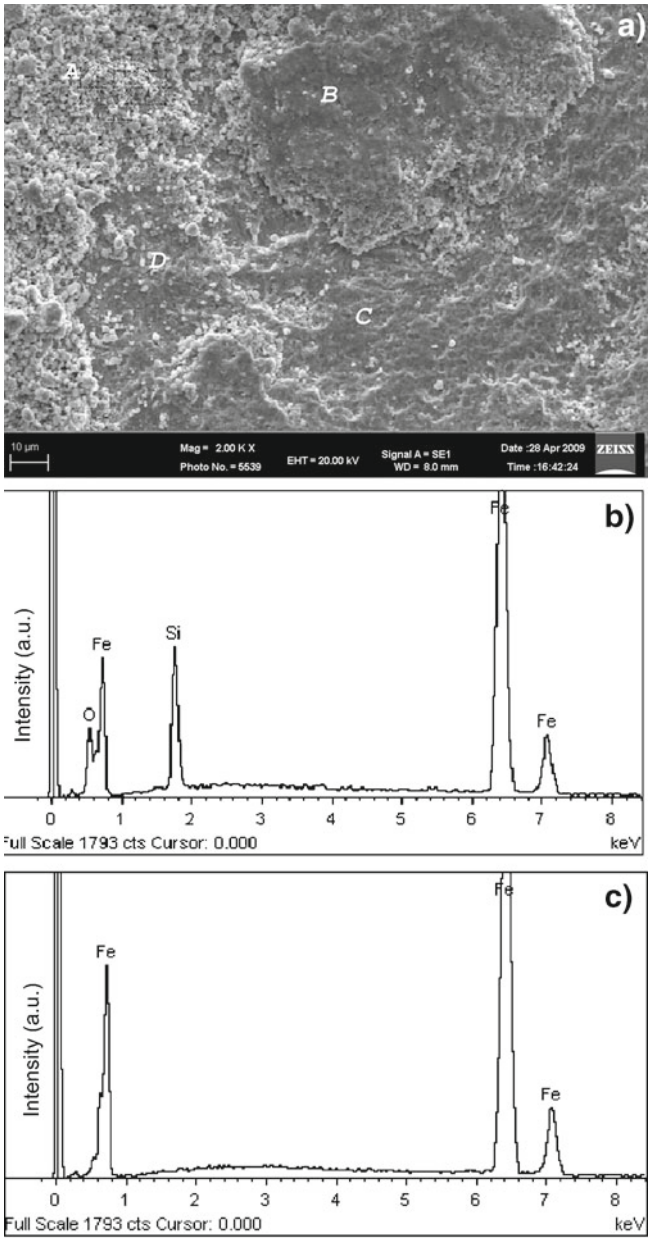

Figure 6. (**a**) Scanning electron micrograph of corroded surface of coating in borate buffer solution of pH-7·7, (**b and c**) EDX patterns from points 'A' and 'C' on surface (data from B and D are also reported in table 2).

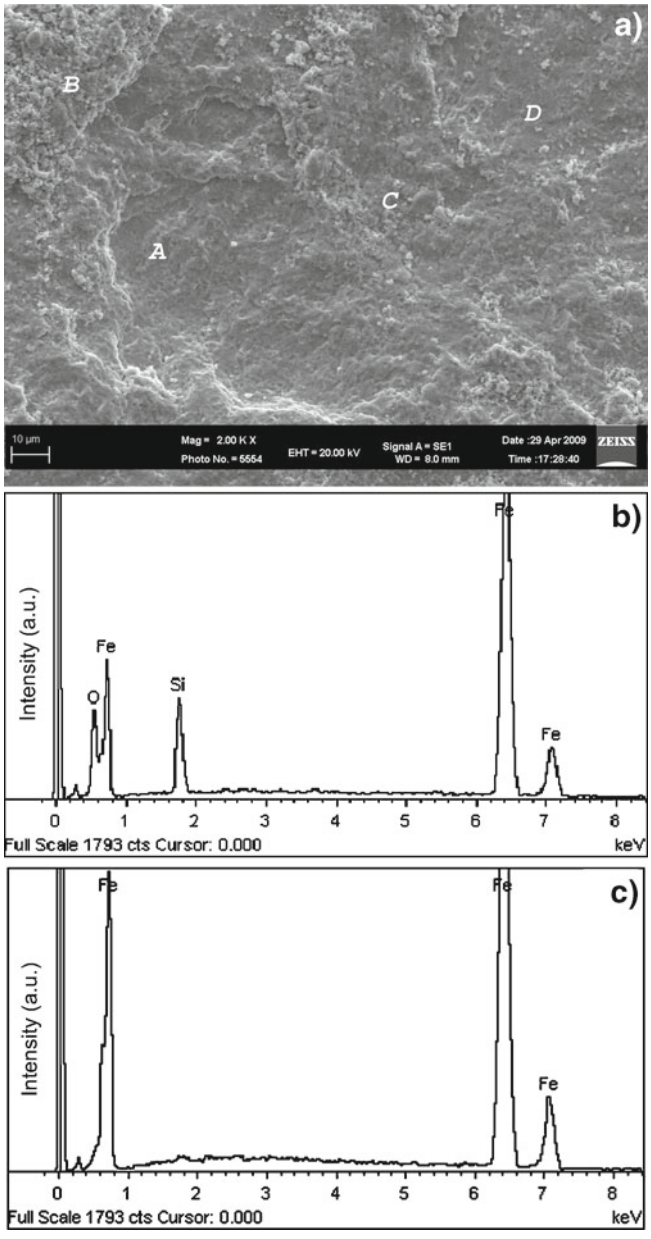

Figure 7. (**a**) Scanning electron micrograph of corroded surface of coating in borate buffer solution of pH-8·4, (**b and c**) EDX patterns at points 'B' and 'D' on surface (data from A and C are also reported in table 2).

Table 2. EDS results obtained on the corroded surfaces in borate buffer solutions.

Sample	Solution	Spectrum	Fe (at%)	Si (at%)	O (at%)
Coating	Borate buffer pH 7·7	A	61·16	10·17	28·68
		B	58·35	18·71	22·95
		C	100		
		D	100		
Coating	Borate buffer pH 8·4	A	100		
		B	65·12	13·74	21·14
		C	52·07	16·75	31·18
		D	100	–	–
Cast $Fe_{80}Si_{20}$		A	77·97	22·03	
		B	79·03	20·97	
		C	78·54	21·46	
		D	78·93	21·07	

completely from the surface rather they get redeposited back on the substrate surface due to the process of ball milling (Gupta *et al* 2009). This effect leads to the formation of Fe or Fe-rich zone. Si can also diffuse into the chipped off Fe particles leading to the formation of Fe-rich regions. Figures 6(b) and (c) show EDX patterns obtained at points A and C, respectively on the surface indicating the presence of Fe, Si and oxygen and Fe-rich regions, respectively. Figure 7(a) shows SEM micrograph of the corroded surface of the coating in borate buffer solution of pH 8·4. The surface is similar to the one observed in case of the coating polarized in the solution of pH 7·7, but the penetration depth is more at some regions. Figures 7(b) and (c) show EDX patterns obtained at a point B and D, respectively, on the corroded surface and these show the presence of Fe, Si and oxygen and Fe-rich regions, respectively. Table 2 shows tentative amounts of Fe, Si and oxygen at various points on the surface. EDX results indicate clearly that some regions are enriched with Fe and those regions are possibly pure Fe zones.

Figure 8(a) shows SEM micrograph of the corroded surface of cast Fe–Si alloy in borate buffer solution of pH 8·4. The surface does not contain any regions enriched with pure Fe and the base composition of the alloy ($Fe_{80}Si_{20}$) is maintained throughout the surface as observed from EDX results (table 2). Figure 8(b) shows an EDX pattern observed at a point 'A' on the surface of the corroded sample. 10–15 spots have been taken for EDX measurement. However, results of only four representative spots are shown in table 2.

The potentiodynamic polarization behaviour shows two types of passive layers in the solution of pH 8·4 and single stable layer in the solution of pH 7·7 as seen in figure 4. However, the substrate shows single passive layer and that too with a much lower current density. So, it clearly suggests that the nature of the substrate does not interfere with the behaviour of the coating in both the solutions. Thus, it confirms that the polarization behaviour of the coating tested in two different pH values is the characteristic of the coating. Formation of two passive layers in the solution of pH 8·4 could possibly be attributed to the formation of different hydroxides and oxides of Fe (Flis *et al* 2009; Díez-Pérez *et al* 2001). It could be attributed to the dissolution of Fe from Fe-enriched regions as seen in the SEM micrographs as shown in figures 6 and 7 and in table 2 and this leads to the formation of second passive layer in the buffer solution of pH 8·4. Formation of two stage passivity was found in case of pure iron in the solution of pH 8·4 in the present case and noted in figure 5, but, the passive current density of second passive layer of the coating is less. This could be attributed to the possible formation of local galvanic cell between the Fe-rich region and regions with 20 at% Si content. Earlier it has been shown that passivation is a strong function of Si content in cast Fe–Si alloy (Wolff *et al* 2001). Self-passivation is hindered if Si is lower than 14 wt% (Omurtag and Doruk 1970; Wolff *et al* 2001). Interestingly, cast $Fe_{80}Si_{20}$ alloy shows single passive layer in the same solution (figure 5) which also gives further support to the mechanism of Fe dissolution from the Fe-enriched localized regions of the coating.

Several theories have been proposed for the occurrence of this type of behaviour of Fe in borate buffer solution of pH 8·4. A study (Flis *et al* 2009) has reported different reactions taking place in the Fe system in the borate buffer solution of pH 8·4 to explain double stage passivity. Dissolution of Fe^{2+} ions and the formation of hydroxides of Fe during the early stages of passivation are observed (Díez-Pérez *et al* 2001). Formation of Fe (II) hydroxide results in oversaturation of the iron cations at the most active sites. Thus, the iron dissolution and formation of its corresponding hydroxides is able to proceed over the whole surface at higher potentials in the active–passive region. This process continues until all the surface is covered, thus, producing effective protection of the iron electrode (Díez-Pérez *et al* 2001). Hence, it proves that the two stage passivation shown by the coating in borate buffer solution of pH 8·4 must be related to Fe-enriched localized regions.

It is clear from the above discussion that the formation of two stage passivity of Fe–Si coating in borate buffer solution of pH 8·4 is related to the Fe-enriched sites on the

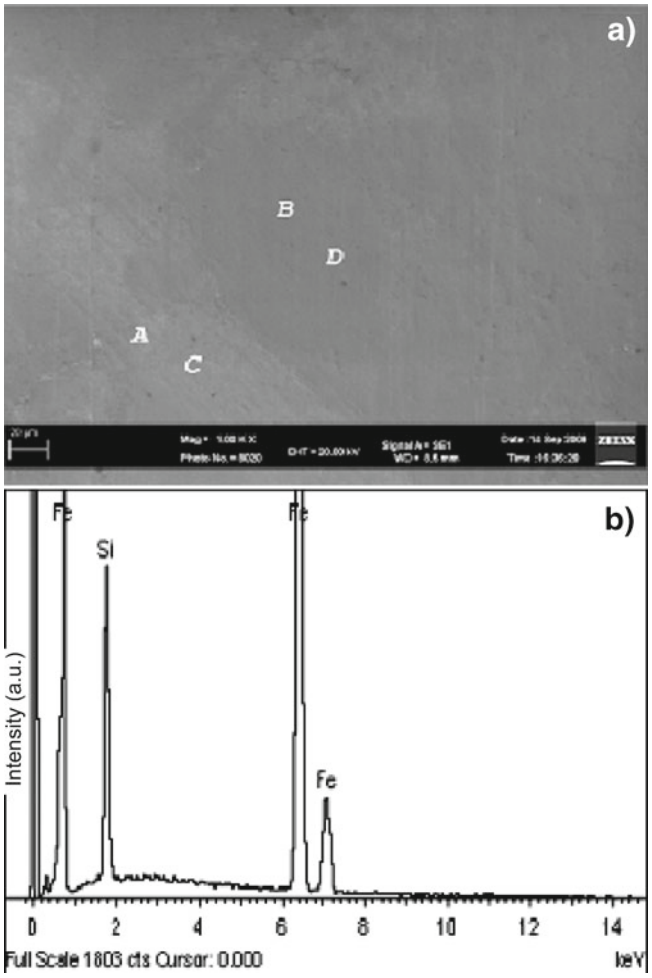

Figure 8. (**a**) Scanning electron micrograph of corroded surface of cast Fe–Si alloy in borate buffer solution of pH 8·4 and (**b**) EDX pattern at point 'A' on surface (data from B, C and D are also reported in table 2).

surface. Though EDX results show no traces of any other elements at some of the regions except iron (100%), there could be a chance of formation of Fe–Si regions with much lower Si content than 20 at% due to inter-diffusion. Hence two stage passivity is attributed to the highly enriched iron regions or the regions with very low Si presence. The actual polarization behaviour of $Fe_{80}Si_{20}$ coating is not reflected due to the presence of Fe-rich regions. So, in order to study the exact behaviour of the nanocrystalline coating, the Fe-enriched sites have to be removed or its formation should be restricted during processing. Further, the growth and dissolution of the passive film is dynamic and the passive current density or corrosion rate changes with time during potentiodynamic polarization measurement, hence it cannot be used accurately as quantitative guidelines for long term corrosion resistance. The sample can develop different conditions over the periods and these conditions cannot be duplicated easily with the short term laboratory experiments. However, potentiodynamic anodic polarization can provide useful preliminary guidelines. In addition to these, presence of trace impurities and their effects on corrosion properties cannot be ignored. It has often been observed that the materials with impurities such as sulphur and phosphorus corrode faster. This is due to low hydrogen overvoltage of their compounds with iron reducing anodic potential and destabilizing passive layer. For example, sulphur combines with iron to form iron sulphides and forms centre of corrosion attack. These are good conductors and stimulate local corrosion cells by acting as strong cathodes. Such attack around sulphide area is so intense that the sulphides fall out of the surface and leads to pitting. It has also been reported that manganese counteracts the bad effect of sulphides as MnS has low conductivity and counter corrosion attack (Wranglen 1969).

4. Conclusions

There is a formation of stable passive layer on the nanocrystalline $Fe_{80}Si_{20}$ coating in borate buffer solution of pH-7·7 whereas two passive layers are formed in the borate buffer solution of pH-8·4. The appearance of two passive layers is due to the dissolution of the localized highly enriched iron regions in the coating and formation of different hydroxides at pH-8·4. Absence of second passive layer and only single passive layer is observed in case of cast Fe–Si alloy as there is no free pure Fe present on the surface. Hence, the polarization behaviour of the coating is highly affected by the highly enriched Fe sites present on the surface.

Acknowledgements

This work has been supported by the Department of Science and Technology, India based on a SERC Engineering Sciences project "Bulk Metallic Glass Coating".

References

Díez-Pérez I, Gorostiza P, Sanz F and Müller C 2001 *J. Electrochem. Soc.* **B148** 307
Ding J, Li Y, Chen F, Deng C, Shi Y, Chow Y and Gang T 2001 *J. Alloys Compd* **314** 262
Flis J, Flis-Kabulska I and Zakroczymski T 2009 *Electrochim. Acta* **54** 1810
Froes F, Senkov O and Baburaj E 2001 *Mater. Sci. Eng.* **A301** 44
Ghosh S, Dey G, Dusane R and Grover A 2006 *J. Alloys Compd* **42** 235
Gupta G, Mondal K and Balasubramaniam R 2009 *J. Alloys Compd* **482** 118
Huang J, Tsai Z and Yu G 2002 *Surf. Coat. Technol.* **202** 4992
Ji G, Elkedimc O and Grosdidier T 2005 *Surf. Coat. Technol.* **190** 406
Li W and Li C 2010 *Appl. Surf. Sci.* **256** 2193
Lu H, Li Y and Wang F 2006 *Thin Solid Films* **510** 197
Meng G, Li Y and Wang F 2006 *Electrochim. Acta* **51** 4277
Omurtag Y and Doruk M 1970 *Corros. Sci.* **10** 225
Pourbaix M 1966 *Atlas of electrochemical equilibria in aqueous solutions*, 1st ed. (Oxford: Pergamon Press Ltd.) pp 461–462
Suryanarayana C and Koch C 2000 *Hyperfine Interact.* **130** 5

Szewieczek D, Tyrlik-Held J and Paszenda Z 1998 *J. Mater. Process. Technol.* **78** 171

Tjong S and Chen H 2004 *Mater. Sci. Eng.* **R45** 1

Wang L, Zhang J, Gao Y, Xue Q, Hua L and Xua T 2006 *Scr. Mater.* **55** 657

Wolff U, Schneider F and Mummert K 2001 in *Electrochemical properties of passive layers on Fe–Si alloys* in *Passivity of metals and semiconductors* (eds) M Ives *et al* (New Jersey: The Electrochemical Society) pp 194–200

Wranglen G 1969 *Corros. Sci.* **9** 585